Fracture Mechanics Prediction of Fatigue Life of Aluminum Highway Bridges

Søren Rom
MSc Eng.
Bridges, COWI A/S
DK-2800 Kgs. Lyngby
Denmark

Henning Agerskov
Professor emeritus
Dept. of Civil Engrg.
Tech. Univ. of Denmark
DK-2800 Kgs. Lyngby
Denmark

Abstract

Fracture mechanics prediction of the fatigue life of aluminum highway bridges under random loading is studied. The fatigue life of welded joints has been determined from fracture mechanics analyses and the results obtained have been compared with results from experimental investigations. The fatigue life of welded plate specimens has been investigated. Both the fracture mechanics analyses and the fatigue tests have been carried out using load histories, which correspond to one week's traffic loading, determined by means of strain gauge measurements on the deck structure of the Farø Bridges in Denmark. The results obtained from the fracture mechanics analyses show a significant difference between constant amplitude and variable amplitude results. Both the fracture mechanics analyses and the results of the fatigue tests carried out indicate that Miner's rule, which is normally used in the design against fatigue in aluminum bridges, may give results which are unconservative. Furthermore, it was in both investigations found that the validity of the results obtained from Miner's rule will depend on the distribution of the load history in tension and compression.

Keywords: Fracture mechanics; Aluminum; Bridges; Highway bridges; Fatigue; Random loading; Variable amplitude fatigue

1. Introduction

Aluminum is a relatively new material in permanent bridge structures. Aluminum is most commonly used for relatively small bridges, e.g. footbridges and short span road bridges. The low weight is one of the major advantages of aluminum in bridge structures, compared to the other bridge structure materials. Normally, specially developed extruded deck profiles are used in aluminum bridges. By welding the deck profiles together at the top and bottom flanges, an almost ideal isotropic bridge deck structure may be obtained. Main disadvantages in using aluminum for bridge structures are the low modulus of elasticity and the low fatigue strength, compared to steel.

A major concern in the design of aluminum bridges is the fatigue life. One of the problems that have attracted increased attention in recent years is the problem of fatigue damage accumulation. Codes and specifications normally give simple rules, using a Miner summation and based on the results of constant amplitude fatigue tests. Over the years, fatigue test series have been carried through using different types of block loadings, and for these types of loading, Miner's rule has in many cases been found to give reasonable results. However, in a real structure the loading does normally not consist of loading blocks, but the structure is subjected to a stochastic loading, due to traffic, wind, etc. Thus, the need for a better understanding of the fatigue behavior under more realistic fatigue loading conditions is obvious.

The question of the validity of Miner's rule has been the background for a series of research projects on fatigue in aluminum and steel structures, carried out at the Department of Civil Engineering of the Technical University of Denmark over a long period of time. The primary purpose of these projects has been to study the fatigue life of aluminum and steel structures under various types of stochastic loading that are realistic in relation to these types of structures. This paper concentrates on the results of the investigations on aluminum bridges.

The types of loading that are used in the present investigation correspond to one week's traffic loading, determined by means of strain gauge measurements at various locations in the deck structure of the Farø Bridges in Denmark. The present investigation includes both analytical determination of the fatigue life under the actual types of random loading by use of fracture mechanics and fatigue tests on welded plate specimens.

2. Experimental Investigation

The present paper concentrates on the fracture mechanics determination of the fatigue life, and thus only a short mention of the experimental investigation is included. A detailed description of the fatigue tests and the results obtained may be found in Rom and Agerskov (2014).

In the experimental investigation, two types of welded test specimens have been used. Test specimen No. 1 consists of a special extruded profile which is welded to the main plate of the test specimen. This test specimen is shown in Fig. 1. Test specimen No. 2 consists of a traditional extruded T-profile welded to the main plate of the test specimen, see Fig. 2. Test specimen No. 1 is intended to give lower stress concentration at the weld toe than test specimen No. 2.

The material used in the present investigation is Al 6005 T6. The ultimate tensile strength and the 0.2% proof strength for the test specimens were determined to be: f_u = 327 MPa and $f_{0.2}$ = 310 MPa, respectively. Both profiles used are extruded and both are welded to a main plate of thickness 10 mm.

The fatigue tests have been carried out in a fixed test frame with a capacity of ±100 kN. The applied loading in these tests is a central normal force in the main plate. Small eccentricities due to the welding of the test specimens are inevitable in these test series. This results in additional secondary bending stresses at the joint. Strain gauges are used on all test specimens in these series to determine the resulting stresses from normal force and eccentricity moment. Furthermore, the stresses in the most critical areas with respect to fatigue have been determined from finite element analysis. Both constant amplitude and variable amplitude fatigue test series have been carried through in the present investigation.

3. Variable Amplitude Loading

The variable amplitude loading that has been used in the present investigation has been determined from strain gauge measurements on the steel deck structure of the Farø Bridges in Denmark. No similar stress histories measured on aluminum bridges were found at the start of this investigation. The load histories correspond to one week's traffic loading. Strain gauge measurements were taken at 10 different locations in the deck structure. The load histories that have been used in the present investigation were measured by two strain gauges, both placed on the bottom of one of the trapezoidal longitudinal stiffeners of the deck plate. The stiffener chosen is located under the most heavily loaded lane of the motorway. The distance from the measurement area to the simple support of the bridge girder on the nearest bridge pier is approximately 8 m. With a length of the bridge spans of approximately 80 m, this location of the strain gauges means that only local bending effects in the deck structure will be registered, whereas the stresses due to global bending in the bridge girder will be negligible. Strain gauge No. 1 is placed in the middle of the longitudinal stiffener span, which has a length of 4 m. Strain gauge No. 5 is placed at a distance of 0.5 m from one of the transverse diaphragms. This means that the stresses measured by strain gauge No. 1 are primarily tensile stresses, whereas the stresses registered by strain gauge No. 5 are almost equally in tension and compression. Only the extremes of the load history are needed, since the load course between consecutive extremes is considered unimportant. Thus, only the peak values of the stress history, registered by the strain gauges during the measuring period, are stored in the computer.

In order to avoid noise and low, non-damaging stress cycles in the stress history to be used, a truncation is carried out on the directly registered stress history. The truncation level $\Delta\sigma_{th}$ has been determined by use of linear elastic fracture mechanics, on the basis of a choice of the threshold value of the stress intensity factor range, ΔK_{th} = 4.2 $\mathrm{MPa}\sqrt{\mathrm{m}}$. This value was determined from crack growth measurements on the material used.

Figs. 3 and 4 show examples of typical load histories based on the measurements from strain gauges No. 1 and 5, respectively. The load level in each variable amplitude test or analysis is determined from the measured load history by multiplication with a scaling factor. When the load history corresponding to one week's traffic has been simulated, the simulation procedure returns to the beginning of the load history and repeats the one week loading.

The main characteristics of the load histories based on the measurements from strain gauges No. 1 and 5 are given in Table 1. The irregularity factor, *I*, is defined as the number of positive-going mean-value crossings divided by the number of maxima of the load history. For narrow band loading, the irregularity factor will be close to unity. Root-mean-square (RMS) and root-mean-cube (RMC) values have been determined from rainflow counts on the load histories. The RMS- and RMC-values given in Table 1 correspond to a maximum stress range in the stress history, $\Delta\sigma_{max} = 1$.

4. Fracture Mechanics Prediction of Fatigue Life

The fatigue life of welded joints can be determined theoretically by the use of fracture mechanics. Of special importance for the validity of the results that are obtained from the fracture mechanics analysis is the consideration of crack closure in the analytical model.

The crack growth analysis model used in the present investigation is based on the Dugdale-Barenblatt strip yielding assumption, with modifications to allow plastically deformed material to be left along the crack surfaces as the crack grows. The crack closure model accounts for load interaction effects, such as retardation and acceleration, under variable amplitude loading. The model may be used to simulate fatigue crack growth under both constant amplitude and variable amplitude loading taking into account the influence of crack closure upon fatigue crack growth. Furthermore, in the determination of the crack growth life the effects of stress concentrations and welding residual stresses are included. In the following is given a brief description of the crack growth model and of the most important parameters used in the model.

4.1. Crack Closure

The mechanisms of crack closure have been attributed to plasticity-induced closure, roughness-induced closure and environment-induced closure. Only the plasticity-induced closure is included in the crack closure model used in the present investigation.

Plasticity-induced crack closure is caused by residual plastic deformations in the wake of an advancing crack. During the unloading part of a load cycle, the crack will close (at least partly) before the minimum load level is reached due to the residual plastic elongations, which are left along the crack surfaces as the crack grows. After full unloading, compressive residual stresses will be present in the wake of and ahead of the crack tip. As a result of the closure of the crack during a part of the applied loading range, the driving force for fatigue crack growth is the effective value ΔK_{eff}, which is the part of the total stress intensity factor range, ΔK, where the crack is fully open:

$$\Delta K_{eff} = K_{max} - K_{op} \tag{1}$$

K_{op} is the stress intensity factor representing the value at which the crack is fully open, i.e. when there is no longer crack surface contact behind the physical crack tip during the uploading part of a load cycle.

The fatigue crack growth rate may be presumed to follow a power law of the following form:

$$\begin{aligned} \frac{da}{dn} &= C(\Delta K_{eff}^{m} - \Delta K_{eff,th}^{m}) \qquad \text{for} \quad \Delta K_{eff} \geq \Delta K_{eff,th} \\ \frac{da}{dn} &= 0 \qquad\qquad\qquad\qquad\quad \text{for} \quad \Delta K_{eff} < \Delta K_{eff,th} \end{aligned} \tag{2}$$

where $\Delta K_{eff,th}$ is the effective threshold stress intensity factor range, below which no crack growth takes place, considering the effect of crack closure.

A fictitious crack with half length d, where $d=a+\rho$, is used in the model. a is half the physical crack length, and ρ is the length of the plastic zone. Fig. 5 shows the fictitious crack with half length d.

In the calculations of the fatigue life using the crack closure model, the following assumptions have been made: 1) only one semi-elliptical crack is growing in the plate element; 2) the ratio between the semi-axes of the crack, *a/b*, is constant throughout the calculation; 3) as an approximation for taking strain hardening into consideration, the flow stress σ_o, which is the average value of the yield stress, f_y (the 0.2% proof strength, $f_{0.2}$), and the ultimate tensile strength, f_u, is introduced; and 4) plane stress and plane strain conditions, as well as conditions between these two, are simulated by using a constraint factor α on the tensile yielding at the crack front to approximately account for three-dimensional stress states.

The crack surface displacements, *V*, are obtained by superposition of the solutions for two elastic problems, a crack subjected to remote stress, *S*, and a crack subjected to a uniform stress, σ, applied over a segment of the crack surface.

The crack surface displacement at the center of element *i* can be expressed as:

$$V_i = Sf(x_i) - \sum_{j=1}^{n} \sigma_j g(x_i, x_j) \tag{3}$$

where:

S is the remote applied stress,
$f(x_i)$ is the crack surface displacement at element *i*, due to unit remote applied stress,
σ_j is the uniform stress acting on the crack surface of element *j*,
$g(x_i, x_j)$ is the crack surface displacement at element *i* due to unit stress acting on element *j*,
n is the number of elements.
Fig. 6 shows the loading and the coordinate system used in the crack closure model. The expression in Eq. 3 is used to determine the contact stresses, σ_j, which are directly related to the crack opening stress, S_o.
The crack extension is simulated at the moment of maximum applied stress. The amount of crack extension, Δa^* is chosen as: $\Delta a^*=0.01\rho_{max}$, where ρ_{max} is the size of the plastic zone caused by the maximum applied stress during the Δa^* growth increment. ρ_{max} may be calculated by using Dugdale's small scale yielding solution:

$$\rho_{Dug} = \frac{\pi}{8}\left(\frac{K_{max}}{\alpha\sigma_o}\right)^2 \tag{4}$$

where K_{max} is the maximum stress intensity factor, and α is the constraint factor on tensile yielding.

4.2. Residual Stresses

In the present model, the stress intensity factor at the crack tip is determined by linear superposition of the stress intensity factor due to the applied load and to the residual stress field. The residual stresses at the weld, σ_r, cf. Fig. 7, are taken into account by transforming the residual stress field into an equivalent, remote uniform stress S_{eq}, which results in the same stress intensity factor at the crack tip, as the residual stress field. This transformation gives the following equivalent stress:

$$S_{eq} = \frac{2}{F_G\pi}\int_0^a \frac{\sigma_r(x)}{\sqrt{a^2 - x^2}}dx \tag{5}$$

where $\sigma_r(x)$ is the welding residual stress distribution in the uncracked body at the line of potential crack growth.

4.3. Stress Intensity Factor

In the analysis of the fatigue life, it is assumed that a single crack propagates in a semi-elliptical shape from the weld toe. Most cracked specimens from the fatigue tests of the present investigation showed sign of such a propagation stemming from a single crack; but in some cases it was observed that two or more cracks grew together and resulted in a single crack at an early stage.

A widely used approximate calculation of the stress intensity factor for a surface semi-elliptical crack in a structural detail is obtained by using the method proposed by Albrecht and Yamada (1977). Using this method, *K* is expressed as follows:

$$K = F_S \cdot F_E \cdot F_T \cdot F_G \cdot S \cdot \sqrt{\pi a} \tag{6}$$

where F_S, F_E, F_T and F_G are correction factors for free surface, elliptical crack shape, finite plate thickness or width, and geometry or stress gradient, respectively. The stress intensity factor corrections, F_S, F_E, and F_T may be found from Tada, Paris, and Irwin (1973), Albrecht and Yamada (1977), Fatigue Handbook (1985) and Broek (1986). F_G may be determined from the results of a finite element analysis using the weight function method. S is the remote applied stress.

4.4. Parameters Used in Fracture Mechanics Analysis

In the following, the most important parameters used in the fracture mechanics analysis are discussed, and the actual values of the parameters are given. The crack growth coefficients, m and C, in Eq. 2 were determined from crack growth measurements carried out on standard Compact-Tension (CT) specimens. The actual values of m and C were determined by a linear regression of crack growth rate data using the method of least squares. The following values of m and C were obtained:

$$m = 4.28 \tag{7}$$

$$C = 4.48 \cdot 10^{-12} \ \frac{\mathrm{m}}{(\mathrm{MPa}\sqrt{\mathrm{m}})^{4.28}} \tag{8}$$

The measured crack growth rate as a function of the stress intensity factor range is shown in Fig. 8. Based on the results shown in Fig. 8, the effective threshold stress intensity factor range may be taken as

$$\Delta K_{eff,th} = 4.2 \ \mathrm{MPa}\sqrt{\mathrm{m}} \tag{9}$$

There are considerable uncertainties in the determination of the effective threshold stress intensity factor range. As stated in Pook (1983), the threshold value may be seriously overestimated. The effective threshold stress intensity factor range has been found to be as low as $\Delta K_{eff,th} = 1.0 \ \mathrm{MPa}\sqrt{\mathrm{m}}$. Due to the various uncertainties in the determination of the effective stress intensity factor range, the following value of $\Delta K_{eff,th}$ was used in the crack growth calculations in the present investigation: $\Delta K_{eff,th} = 0 \ \mathrm{MPa}\sqrt{\mathrm{m}}$

Based on the size of the defects in the actual welded joints and on values reported in the literature, Ibsø (1995), Yamada and Nagatsu (1989), and Ibsø and Agerskov (1996), the value of the initial crack depth, a_i, was in the present investigation chosen as: $a_i = 0.1$ mm.

Fatigue failure was in the fracture mechanics analysis defined at a number of cycles, where a crack depth of half the plate thickness had been reached. This choice of a_f was based on observations of the fracture surfaces of the test specimens, where failure had typically occurred at a crack depth of this size, and is in accordance with recommendations in other investigations, e.g. Dijkstra and van Straalen (1997) and Ibsø (1995). However, with so large a crack size, the total number of cycles to failure is insensitive to a slight change in a_f, due to the very fast crack growth at large crack sizes. This was observed both in the tests and in the fracture mechanics analysis. Thus, with a plate thickness of 10 mm, the crack depth, a_f, corresponding to the final or critical crack size was chosen as: $a_f = 5$ mm. In the fatigue tests, the number of cycles to failure was defined as the number of cycles, where the test specimen actually broke.

The crack shape changes, as the crack grows. In the initial stages, the semi-axis ratio, a/c, may be expected to be at its highest, and as the crack advances, it becomes more flat. Crack coalescence may occur at an early stage, leading to only one relatively flat crack. In the analytical model is used as an approximation a constant value of the semi-axis ratio, $a/c = 0.3$, throughout the calculation. This value has been estimated on the basis of measurements carried out in the fatigue tests. The constraint factor on the tensile yielding, α, was in the present investigation chosen as: $\alpha = 1.73$. This value corresponds to Irwin's experimental plane strain constraint factor.

5. Fatigue Test Results

Five fatigue test series have been carried through in the present investigation, three test series with constant amplitude loading and two series with variable amplitude loading. A total of 56 fatigue tests were carried out in these series.

In the results from variable amplitude tests, the stress parameter used is the equivalent constant amplitude stress range, $\Delta\sigma_e$, defined as:

$$\Delta\sigma_e = \left[\frac{\sum_i (n_i \Delta\sigma_i^m)}{N} \right]^{1/m} \quad (10)$$

in which n_i = number of cycles of stress range $\Delta\sigma_i$; $\Delta\sigma_i$ = variable amplitude stress range; N = total number of cycles to failure ($=\Sigma_i n_i$); and m = slope of corresponding constant amplitude S-N line.

For the results obtained in each test series, the data are fitted to an expression:

$$\log N = \log A - m \cdot \log \Delta\sigma \quad (11)$$

by the method of least squares. In Eq. 11, m and A are constants, N is the number of cycles to failure, and $\Delta\sigma$ is the stress range.

As an example of the results obtained in the fatigue tests, the S-N diagram in Fig. 9 shows the results from the test series on test specimen No. 1 under constant amplitude loading (CA-1) with stress ratio R = -1 and variable amplitude loading (VA-1) with the load history from strain gauge No. 5. For the variable amplitude tests, the results are shown both with and without truncation. In Fig. 9, points marked with an arrow correspond to a test with a non-broken test specimen. These points have not been included in the regression analysis.
Further results obtained in the experimental investigation may be found in Rom and Agerskov (2014).

6. Results of Fracture Mechanics Analysis

The fatigue lives have been calculated for the welded plate specimens using the crack growth computer program, FAWS (**F**atigue **A**nalysis of **W**elded **S**tructures), originally developed by J.B.Ibsø, Ibsø (1995) and Ibsø and Agerskov (1996). In the present study, some modifications and optimizations have been implemented in the program.

Calculations have been performed both for constant amplitude loading and for variable amplitude loading. For constant amplitude loading, the analysis has been carried out using the same stress ratios as the ones used in the fatigue tests, R = -1 and R = -1/5. For variable amplitude loading, the calculations have been carried out using the load histories, which were used in the fatigue tests, i.e. the load histories from strain gauges No. 1 and No. 5. The fracture mechanics calculations have been carried out for test specimen No. 1.

In the fracture mechanics determination of the fatigue life, the effect of residual stresses has been investigated. Fatigue life calculations have been carried out using three different levels of the residual stress: 1. Assuming the residual stress to be equal to $+f_y$, 2. Assuming the residual stress to be equal to $+f_y/2$, and 3. Assuming no residual stress. For the yield stress, f_y, the 0.2% proof strength of the actual material, $f_{0.2}$ = 310 MPa has been used.

6.1Constant Amplitude Loading

For constant amplitude loading, R = -1 and R = -1/5, three different sets of calculations have been performed to study the effects of the residual stresses and crack closure. The crack growth lives have been calculated using the above mentioned three levels of residual stresses. The following analyses have been carried out:

Sim CA1-1: Crack growth simulations for constant amplitude loading, R = -1.
Residual stress: $\sigma_r = f_y$

Sim CA1-2: Crack growth simulations for constant amplitude loading, R = -1.
Residual stress: $\sigma_r = f_y/2$

Sim CA1-3: Crack growth simulations for constant amplitude loading, R = -1.
Residual stress: $\sigma_r = 0$

Sim CA2-1: Crack growth simulations for constant amplitude loading, R = -1/5.
Residual stress: $\sigma_r = f_y$

Sim CA2-2: Crack growth simulations for constant amplitude loading, R = -1/5.
Residual stress: $\sigma_r = f_y/2$

Sim CA2-3: Crack growth simulations for constant amplitude loading, R = -1/5.
Residual stress: $\sigma_r = 0$

The results of the crack growth analyses for constant amplitude loading with R = -1 and R = -1/5 are shown in Fig. 10 and 11, respectively. All the results obtained in the simulations for constant amplitude loading may be seen in Fig. 12.

Both Fig. 10 and Fig. 11 show that the *S-N* lines from the crack growth simulations with residual stress equal to f_y and $f_y/2$ are almost identical. A large difference in the level of the stress range is observed, when comparing the *S-N* lines from the crack growth simulations with residual stress equal 0, to the *S-N* lines from the simulations with residual stress equal to f_y and $f_y/2$. The results obtained correspond well with the fact that higher tensile residual stresses should in general give shorter fatigue life.

The *S-N* lines in Fig. 12 clearly show that for constant amplitude loading with residual stress equal to 0, the *S-N* line for R = -1/5 lies lower than the *S-N* line for R = -1. A larger part of the stress range will be in compression for R = -1, and this reduces the crack growth rate and thus gives longer fatigue life than for R = -1/5 at the same stress range level. However, this is not the case for the simulations with residual stress equal to f_y and $f_y/2$. The reason for this is that the compressive part of the stress range is reduced or the stress range is completely in tension, as a result of a higher level of the tensile residual stresses.

6.2Variable Amplitude Loading

For variable amplitude loading, six different sets of calculations have been performed. For each of the two load histories investigated, three different levels of residual stresses have been used. No truncation of small stress ranges in the load histories has been carried out in the simulations. The following analyses were carried through:

Sim VA1-1: Crack growth simulations for variable amplitude loading.
Load history from strain gauge No. 5.
Residual stress: $\sigma_r = f_y$

Sim VA1-2: Crack growth simulations for variable amplitude loading.
Load history from strain gauge No. 5.
Residual stress: $\sigma_r = f_y/2$

Sim VA1-3: Crack growth simulations for variable amplitude loading.
Load history from strain gauge No. 5.
Residual stress: $\sigma_r = 0$

Sim VA2-1: Crack growth simulations for variable amplitude loading.
Load history from strain gauge No. 1.
Residual stress: $\sigma_r = f_y$

Sim VA2-2: Crack growth simulations for variable amplitude loading.
Load history from strain gauge No. 1.
Residual stress: $\sigma_r = f_y/2$

Sim VA2-3: Crack growth simulations for variable amplitude loading.
Load history from strain gauge No. 1.
Residual stress: $\sigma_r = 0$

The results obtained in the simulations for variable amplitude loading with the load histories from strain gauge No. 5 and No. 1 are shown in Fig. 13 and Fig. 14, respectively. All the results obtained in the simulations for variable amplitude loading may be seen in Fig. 15.

Both Fig. 13 and Fig. 14 show that the *S-N* lines from the crack growth simulations with residual stress equal to f_y and $f_y/2$ are almost identical. A larger difference in the level of the stress range is observed, when comparing the *S-N* lines from the crack growth simulations with residual stress equal to 0, to the *S-N* lines from the simulations with residual stress equal to f_y and $f_y/2$. This corresponds well with the fact that higher tensile residual stresses should in general give shorter fatigue life.

The *S-N* lines in Fig. 15 clearly show that for variable amplitude loading with the residual stress equal to 0, the *S-N* line for the load history from strain gauge No. 5 lies higher than the *S-N* line for the load history from strain gauge No. 1. A larger part of the stress range will be in compression for strain gauge No. 5, and this reduces the crack growth rate and thus gives longer fatigue life than for strain gauge No. 1 at the same stress range level. This is also the case for the simulations with the residual stress equal to f_y and $f_y/2$. For the simulations with residual stress equal to f_y and $f_y/2$, the *S-N* lines for the two load histories tend to meet at a high number of cycles.

7. Observations

7.1. Comparison of Results from Fracture Mechanics Analyses

The *S-N* lines obtained in the simulations for constant amplitude loading and for variable amplitude loading are compared for each of the three levels of residual stresses.

Fig. 16 shows a comparison between the *S-N* lines for constant amplitude loading and for variable amplitude loading, all with the residual stress equal to f_y. Fig. 17 shows a comparison between the *S-N* lines for constant amplitude loading and for variable amplitude loading, all with the residual stress equal to $f_y/2$. Fig. 18 shows a comparison between the *S-N* lines for constant amplitude loading and for variable amplitude loading, all with the residual stress equal to 0.

Figs. 16-18 clearly show that the *S-N* lines for variable amplitude loading lie below the corresponding *S-N* lines for constant amplitude loading. This is the case for all three levels of residual stresses investigated.

The difference in fatigue life at variable amplitude and constant amplitude loading can be quantified by the Miner sum, M, determined as the number of cycles to failure at variable amplitude loading, N_{va}, divided by the number of cycles to failure at constant amplitude loading, N_{ca}, at the same equivalent stress range level. When the slope of the *S-N* lines for variable amplitude loading and for constant amplitude loading are not identical, M will be a function of the stress range level.

Comparing the *S-N* lines, obtained from the simulations with residual stresses of f_y or $f_y/2$ for variable amplitude loading with the load history from strain gauge No. 5, to constant amplitude loading with R = -1, a Miner sum of $M \sim 0.1 - 0.5$ is found. For variable amplitude loading with the load history from strain gauge No. 1 compared to constant amplitude loading with R = -1/5, the Miner sum is even lower.

The cumulative damage rule generally used today in the design of aluminum structures against fatigue, assumes that fracture occurs for a Miner sum of M = 1, see e.g. European Committee for Standardization (2007). The results found in the present investigation indicate that the distribution of the load history in tension and compression has a significant influence on the validity of the results, which are obtained by use of the linear fatigue damage accumulation formula.

7.2. Comparison between Results from Fracture Mechanics Analyses and from Fatigue Tests

In the following, the results obtained in the fracture mechanics analyses are compared to the results from the fatigue tests. For the variable amplitude tests, the results without truncation are used. For constant amplitude loading, the test results are compared to the simulations with the residual stress equal to $f_y/2$. For variable amplitude loading, the test results are compared to the simulations with the residual stress equal to $f_y/2$ and 0.

7.2.1. Constant Amplitude Loading

The results of the simulations and the fatigue test results for constant amplitude loading with R = -1 are shown in Fig. 19. The fatigue test results and the results of the simulations for constant amplitude loading with R = -1/5 are shown in Fig. 20.

From Figs. 19 and 20 it can be seen that a very good agreement is obtained between the results from the fatigue tests and the results from the fracture mechanics analyses. This indicates that the level of the residual stresses in the test specimens has been near the assumed level of $f_y/2$.

7.2.2. Variable Amplitude Loading

The fatigue test results and the results of the simulations for variable amplitude loading with the load history from the Farø Bridges, strain gauge No. 5 are shown in Fig. 21. The fatigue test results and the results of the simulations for variable amplitude loading with the load history from the Farø Bridges, strain gauge No. 1 are shown in Fig. 22.

Fig. 21 shows a good agreement between the test results and the results of the fracture mechanics analyses at a lower number of cycles, if a residual stress of $f_y/2$ is assumed. For a larger number of cycles, the *S-N* line from the tests lie between the two *S-N* lines from the simulations, corresponding to $\sigma_r = 0$ and $\sigma_r = f_y/2$.

In Fig. 22 both simulated *S-N* lines lie below the *S-N* line obtained in the fatigue tests, meaning that the fracture mechanics analyses carried out for this loading resulted in somewhat lower fatigue lives than corresponding to the fatigue tests.

8. Conclusions

An investigation has been carried out to study the fatigue life of aluminum highway bridges under random loading, and comparisons between results of fracture mechanics analyses, experimental results, and results obtained using current codes and specifications, i.e. Miner's rule, are given.

The present paper concentrates on the fracture mechanics determination of the fatigue life. A detailed description of the experimental results has previously been given in Rom and Agerskov (2014).

Five fatigue test series were carried through, using plate test specimens with welded attachments. The fatigue lives of the welded joints were determined theoretically by use of fracture mechanics for both constant amplitude loading and highway bridge loading. A comparison of the results of the fracture mechanics calculations and the experimental results in general shows good agreement, when the calculations are based on estimated, realistic values of the welding residual stresses and crack closure is included.

Both the results of the fracture mechanics calculations and the results from the experimental investigations in general show a significant difference between constant amplitude and variable amplitude results. At higher levels of the stress range, the *S-N* lines for variable amplitude loading are considerably below the corresponding *S-N* lines for constant amplitude loading, resulting in quite low values of the Miner sum. At lower levels of the stress range, less difference between the *S-N* lines was observed. However, in all cases the Miner sums which were obtained from the fracture mechanics calculations are less than 1.0.

On the basis of the results obtained, it can be concluded from both the fracture mechanics analyses and the experimental investigations that Miner's rule may give quite unconservative predictions of the fatigue life. This was especially found to be the case for load histories with stress distributions, which are almost equally in tension and compression. These results indicate that the distribution of the load history in tension and compression has a significant influence on the validity of the results, which are obtained by use of Miner's rule.

Acknowledgments

This investigation is a part of a larger research program on the fatigue life of aluminum and steel structures under various types of random loading. The funding for the present investigation has been provided by Skan Aluminium, the Technical University of Denmark, and Hydro Aluminium, who are gratefully acknowledged. The permission from the Road Directorate, Danish Ministry of Transport to carry out the strain gauge measurements on the Farø Bridges is greatly appreciated.

References

Albrecht, P., and Yamada, K. (1977). "Rapid calculation of stress intensity factors." J. Struct. Div., ASCE, 103(2), 377-389.

Broek, D. (1986). Elementary Fracture Mechanics, fourth revised edn., Martinus Nijhoff Publishers, The Netherlands.

Dijkstra, O. D., and van Straalen, I. J. J. (1997). "Fracture mechanics and fatigue of welded structures." Proc., Int. Conf. on Perf. of Dynamically Loaded Welded Struct., S. J. Maddox and M. Prager, eds., Welding Research Council, New York, 225-239.

European Committee for Standardization (CEN). (2007). “Eurocode 9: Design of aluminium structures - Part 1-3: Structures susceptible to fatigue.” EN 1999-1-3:2007, Brussels, Belgium.

Fatigue handbook - Offshore steel structures. (1985). A. Almar-Næss, ed., Tapir Publishers, Trondheim, Norway.

Ibsø, J. B. (1995). "Fatigue life prediction of welded joints based on fracture mechanics and crack closure". PhD thesis, Rep. No. R 322, Technical University of Denmark, Lyngby, Denmark.

Ibsø, J. B., and Agerskov, H. (1996). "An analytical model for fatigue life prediction based on fracture mechanics and crack closure." J. Constr. Steel Res., 37(3), 229-261.

Pook, L. P. (1983). The role of crack growth in metal fatigue, The Metals Society, London, England.

Rom, S., and Agerskov, H. (2014). “Fatigue in Aluminum Highway Bridges under Random Loading”, International Journal of Applied Science and Technology, Philadelphia, Pa, USA, Vol. 4, No. 6, 95-107.

Tada, M., Paris, P. C., and Irwin, G. R. (1973). The stress analysis of cracks handbook. Del Research Corporation, Hellertown, Pa, USA.

Yamada, K., and Nagatsu, S. (1989). "Evaluation of scatter in fatigue life of welded details using fracture mechanics". Struct. Engrg./Earthquake Engrg., 6(1), 13-21.

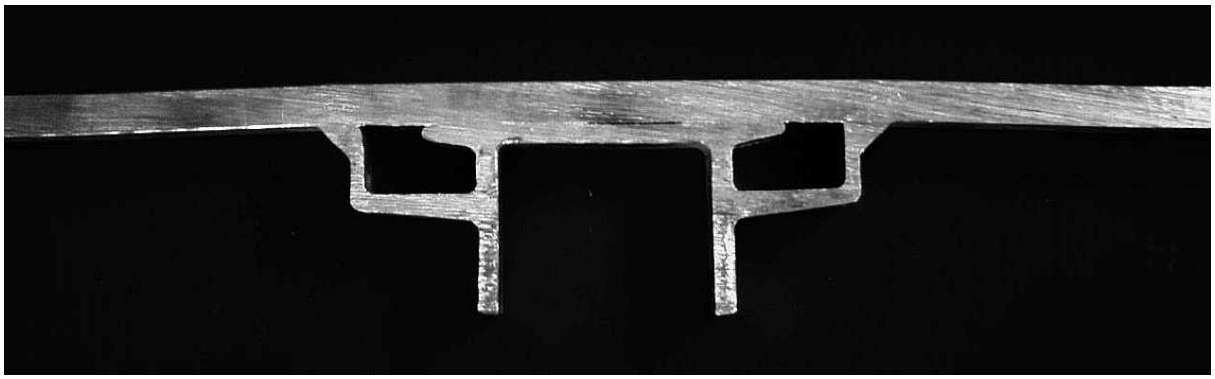

Figure 1: Test Specimen No. 1

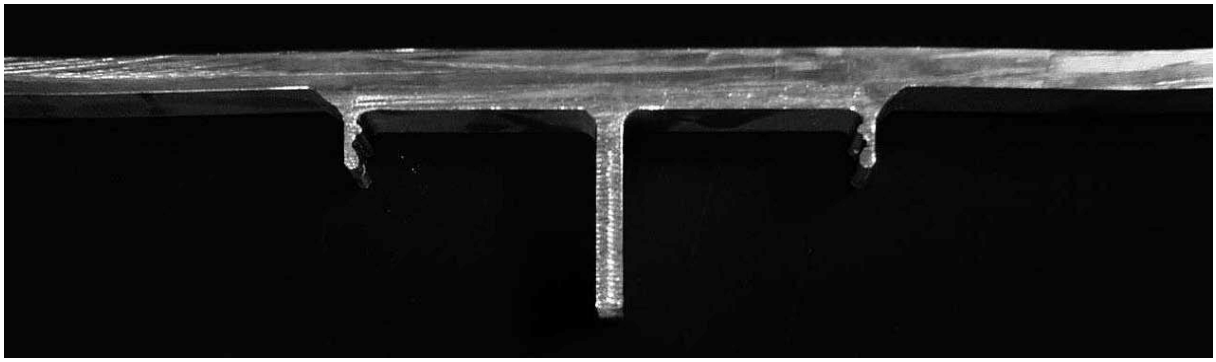

Figure 2: Test Specimen No. 2

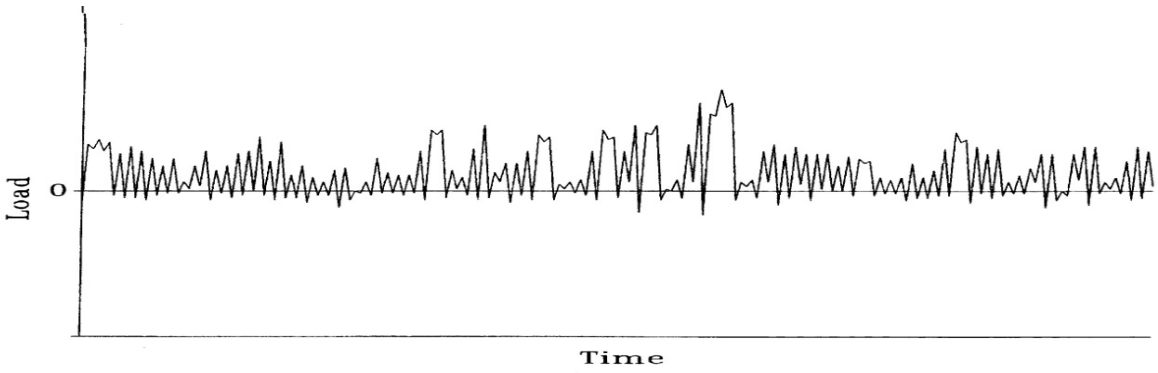

Figure 3: Example of Load History. 200 Extremes Based on the Measurements from Strain Gauge No. 1

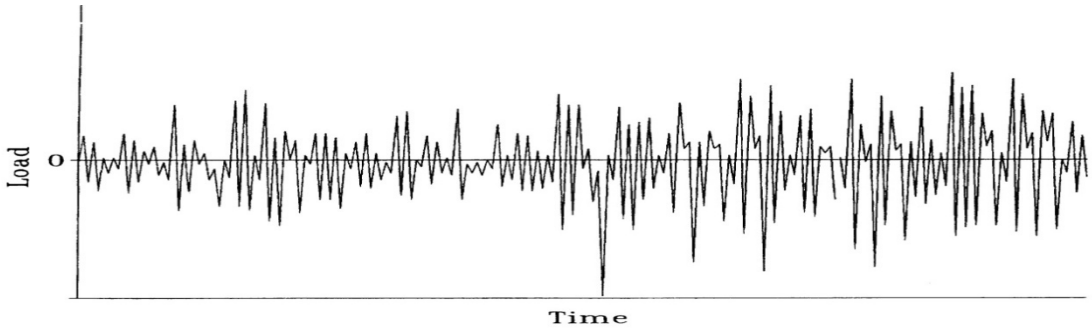

Figure 4: Example of Load History. 200 Extremes Based on the Measurements from Strain Gauge No. 5

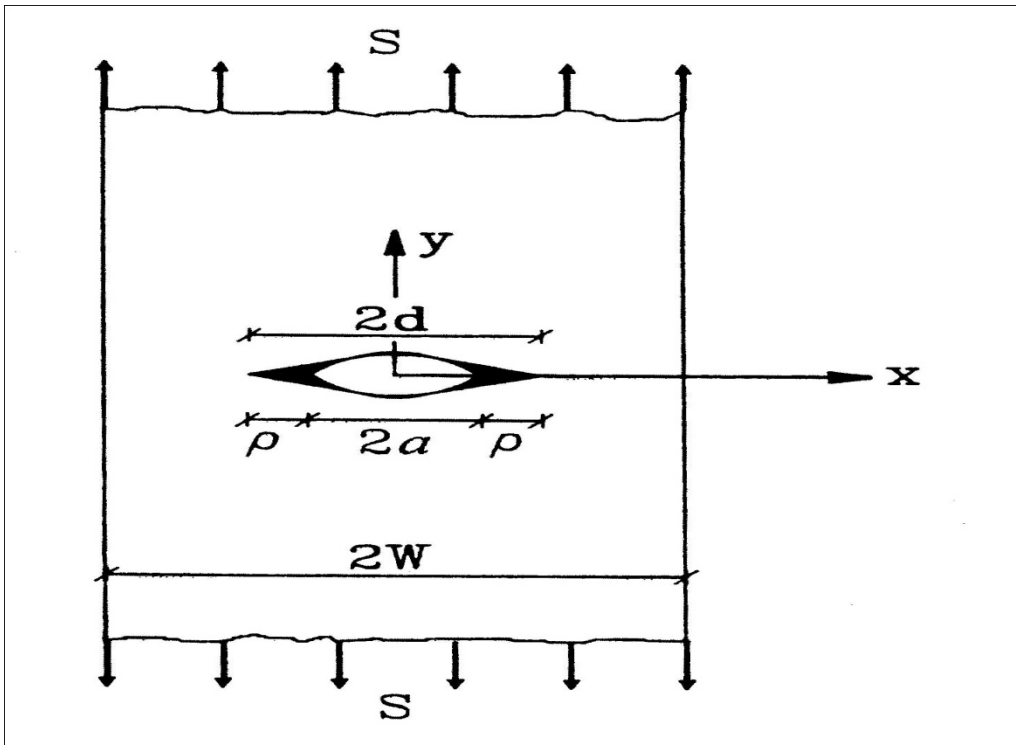

Figure 5: Fictitious Crack with Dugdale Plastic Zone ρ

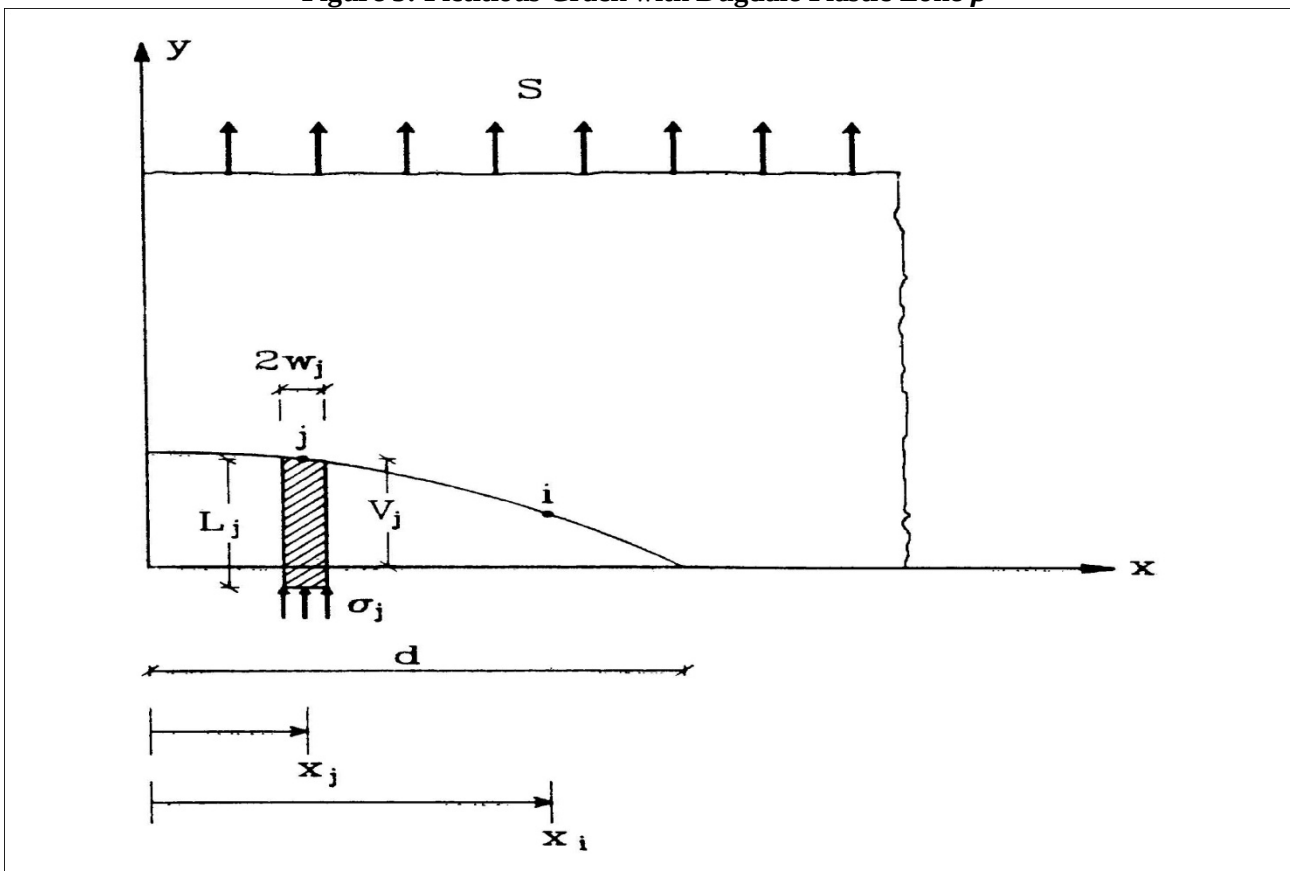

Figure 6: Schematic Loading and Coordinate System Used in Crack Closure Model

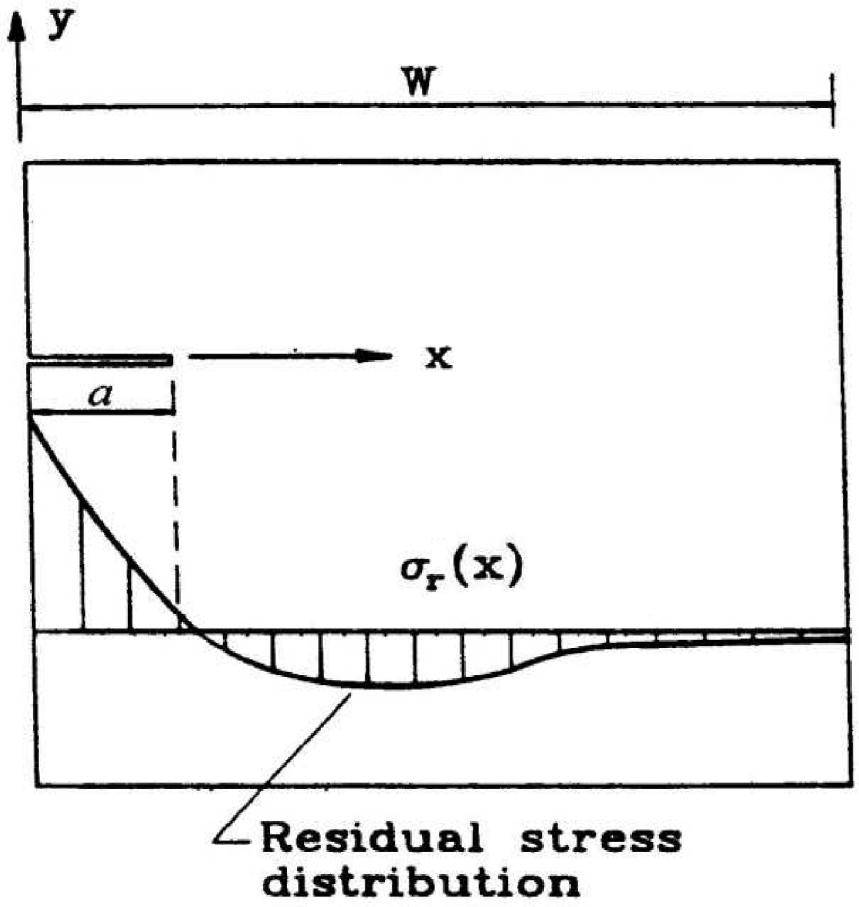

Figure 7: Crack Growth in a Residual Stress Field

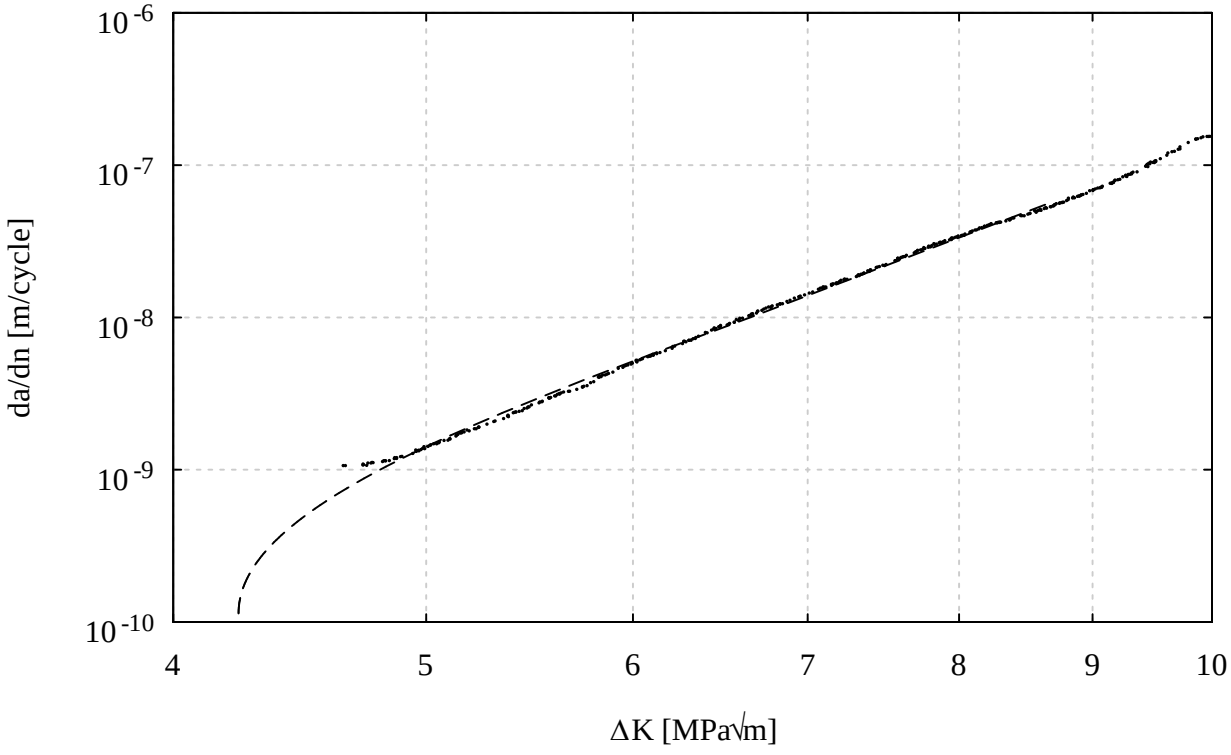

Figure 8: Crack Growth Rate versus Stress Intensity Factor Range

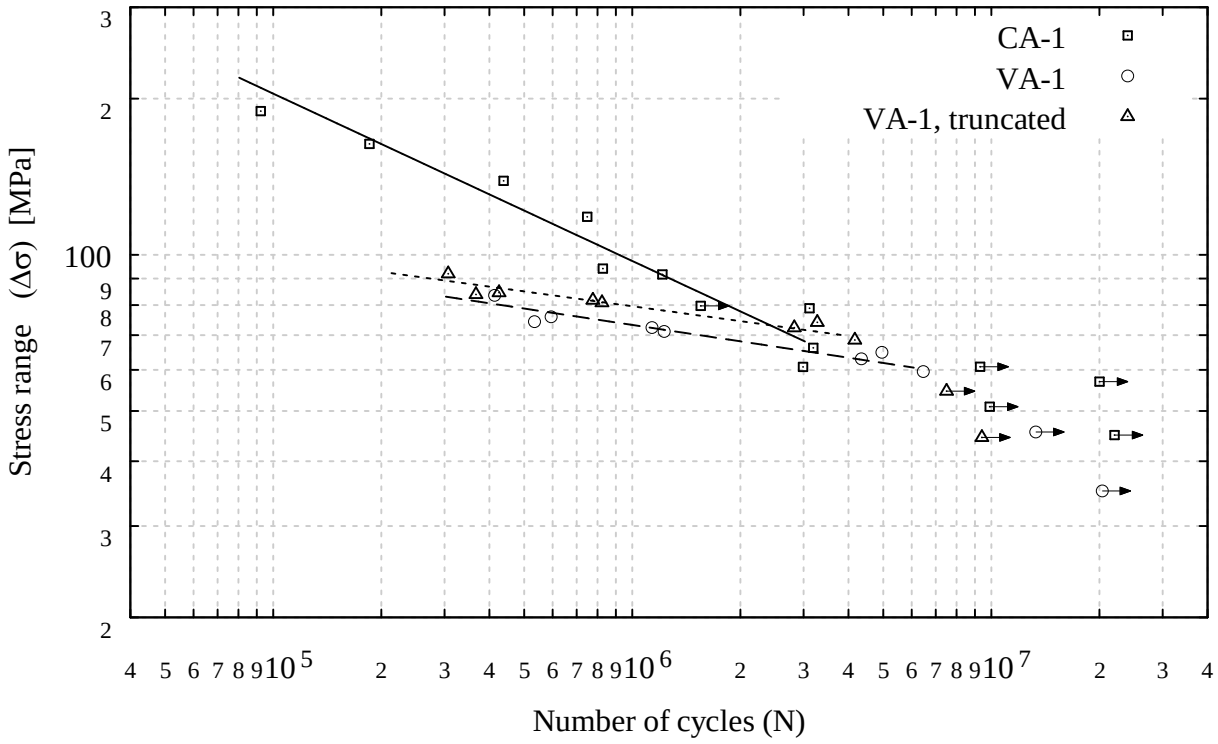

Figure 9: Results of Constant Amplitude Tests (CA-1), *R* = -1, and Variable Amplitude Tests (VA-1) with Load History from Strain Gauge No. 5. Test Specimen No. 1

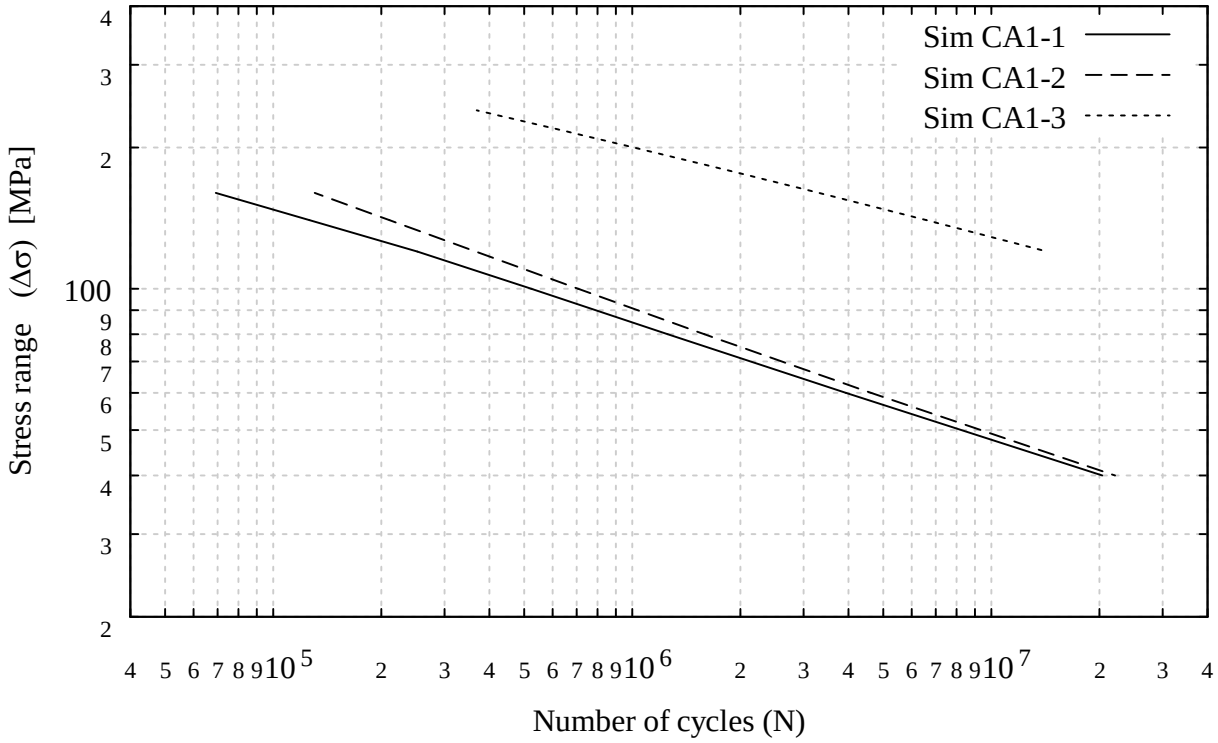

Figure 10: Comparison between Calculated Fatigue Lives; Constant Amplitude Loading, *R* = -1

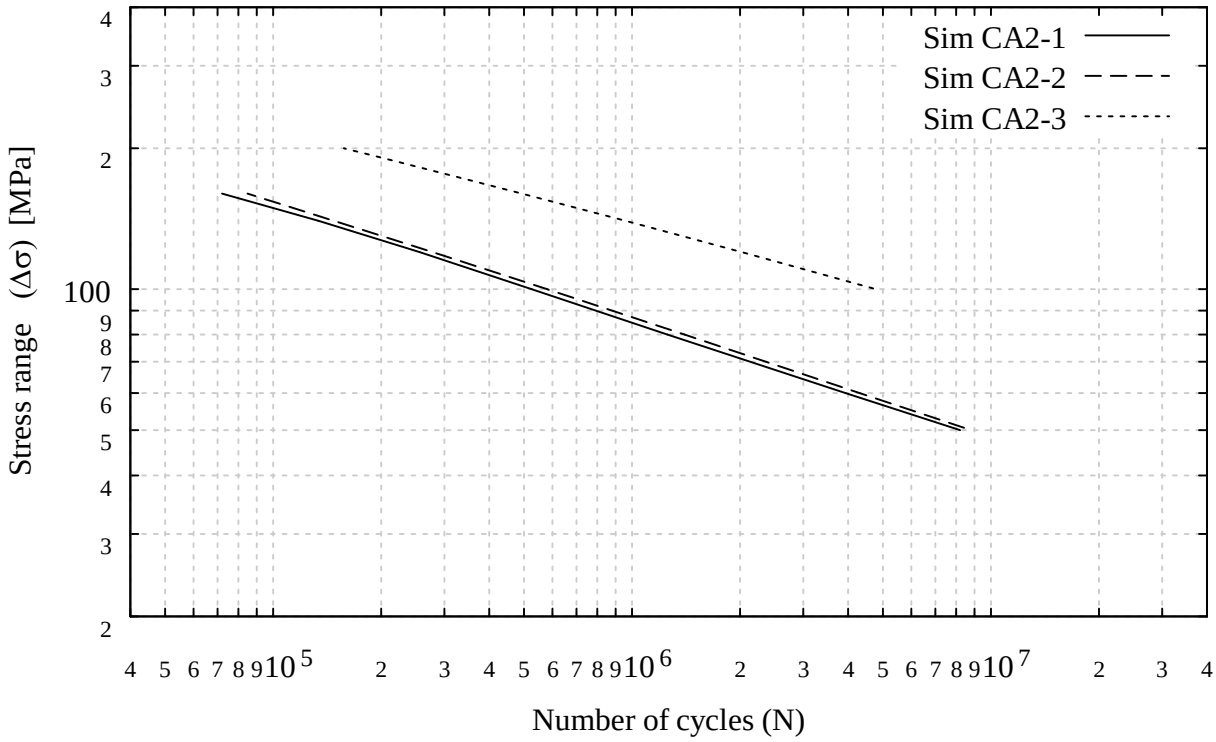

Figure 11: Comparison between Calculated Fatigue Lives; Constant Amplitude Loading, *R* = - 1/5

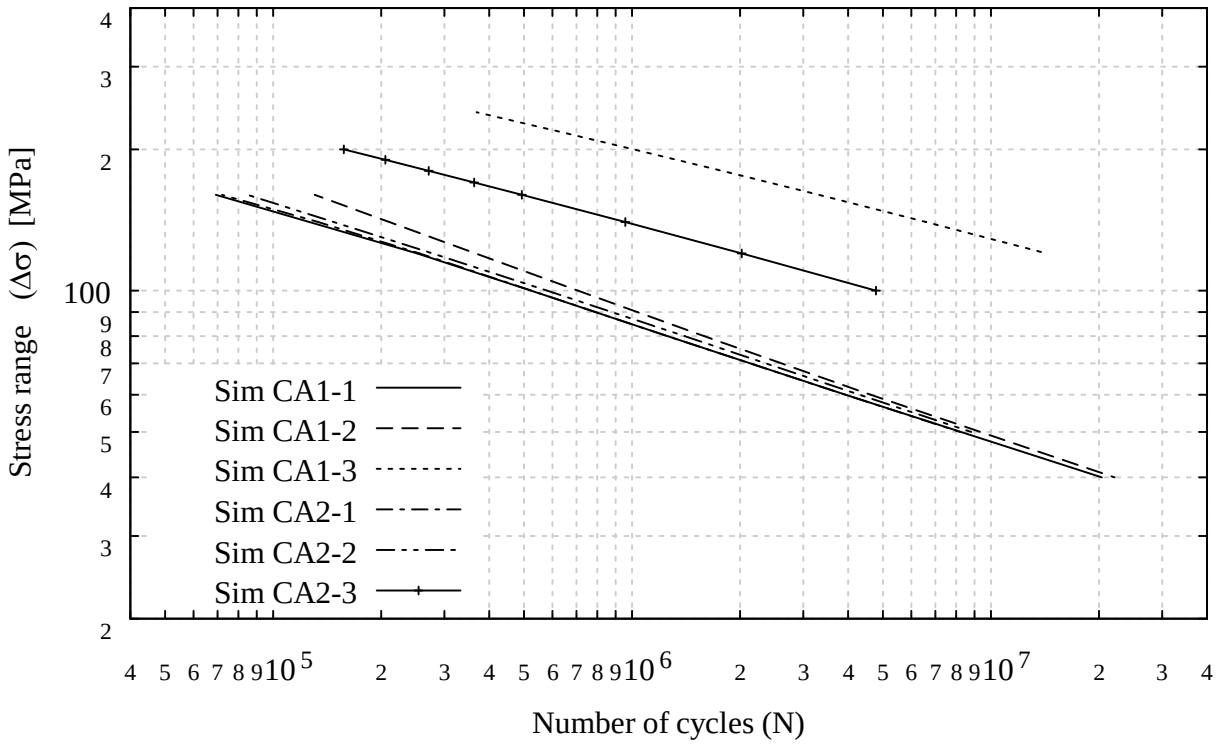

Figure 12: *S-N* Lines Obtained in Simulations for Constant Amplitude Loading, *R* = -1 and *R* = - 1/5

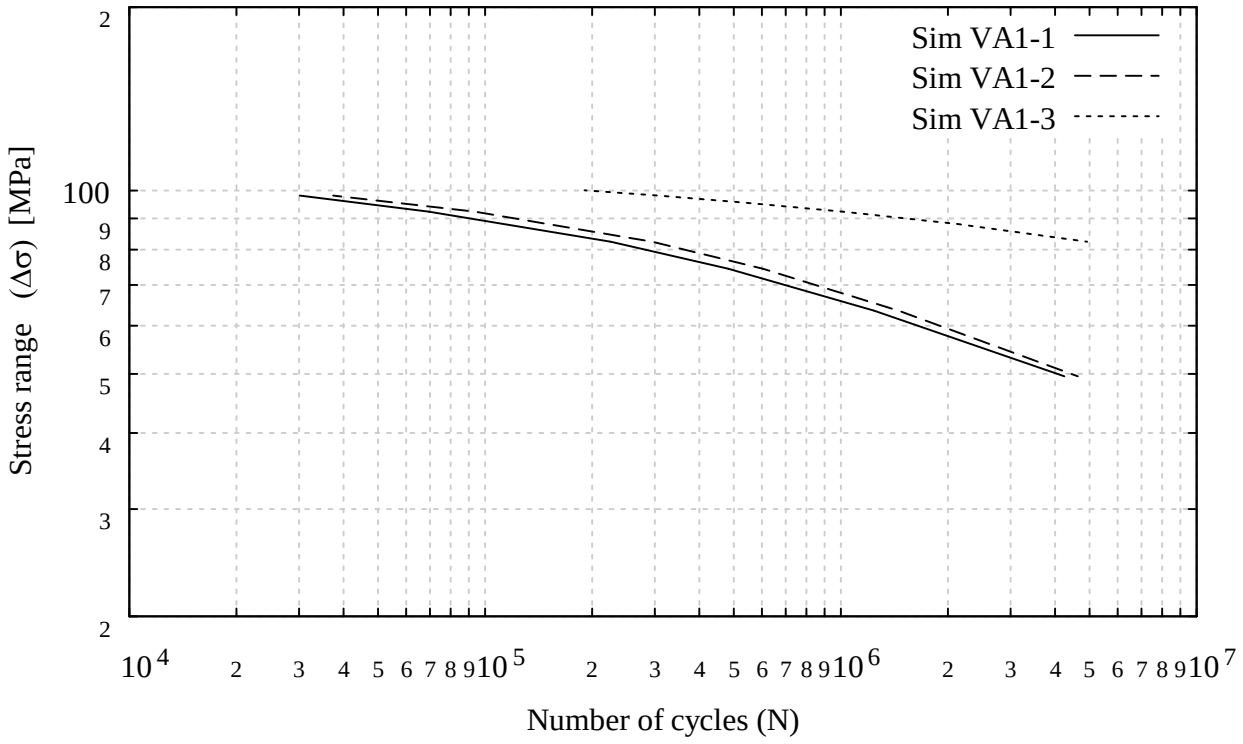

Figure 13: Comparison between Calculated Fatigue Lives; Variable Amplitude Loading, Load History from Strain Gauge No. 5

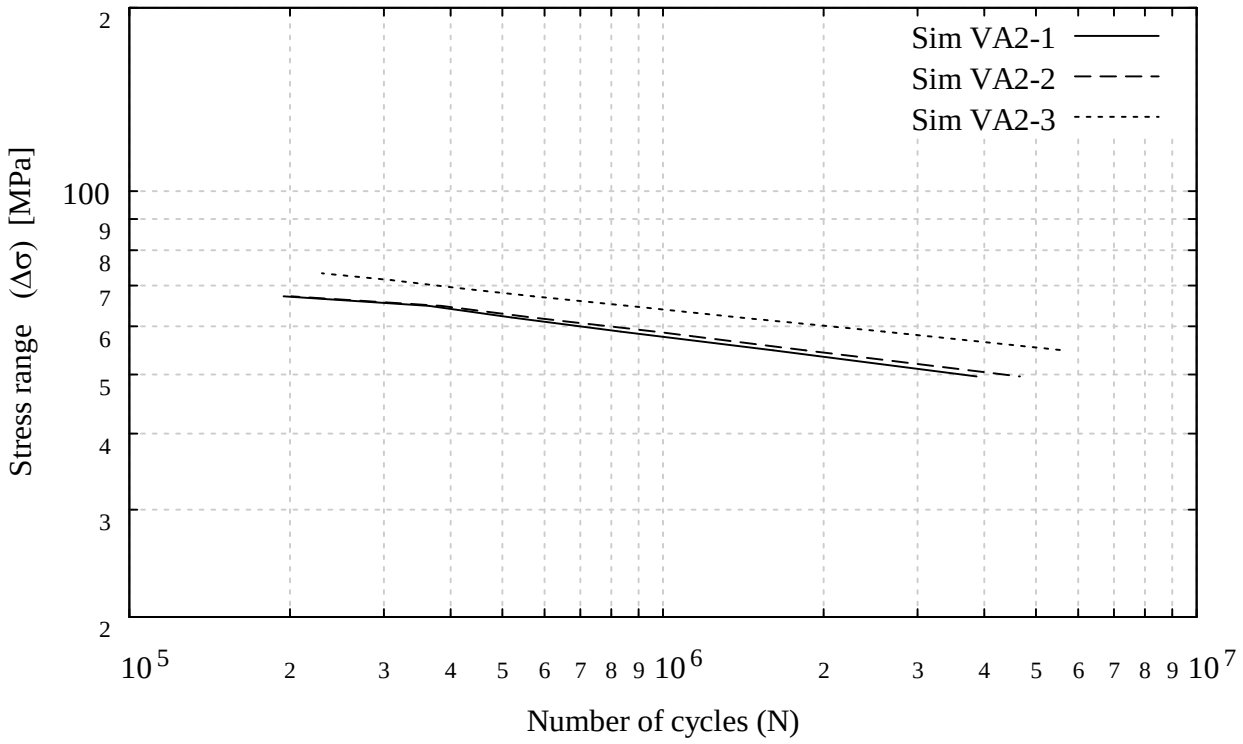

Figure 14: Comparison between Calculated Fatigue Lives; Variable Amplitude Loading, Load History from Strain Gauge No. 1

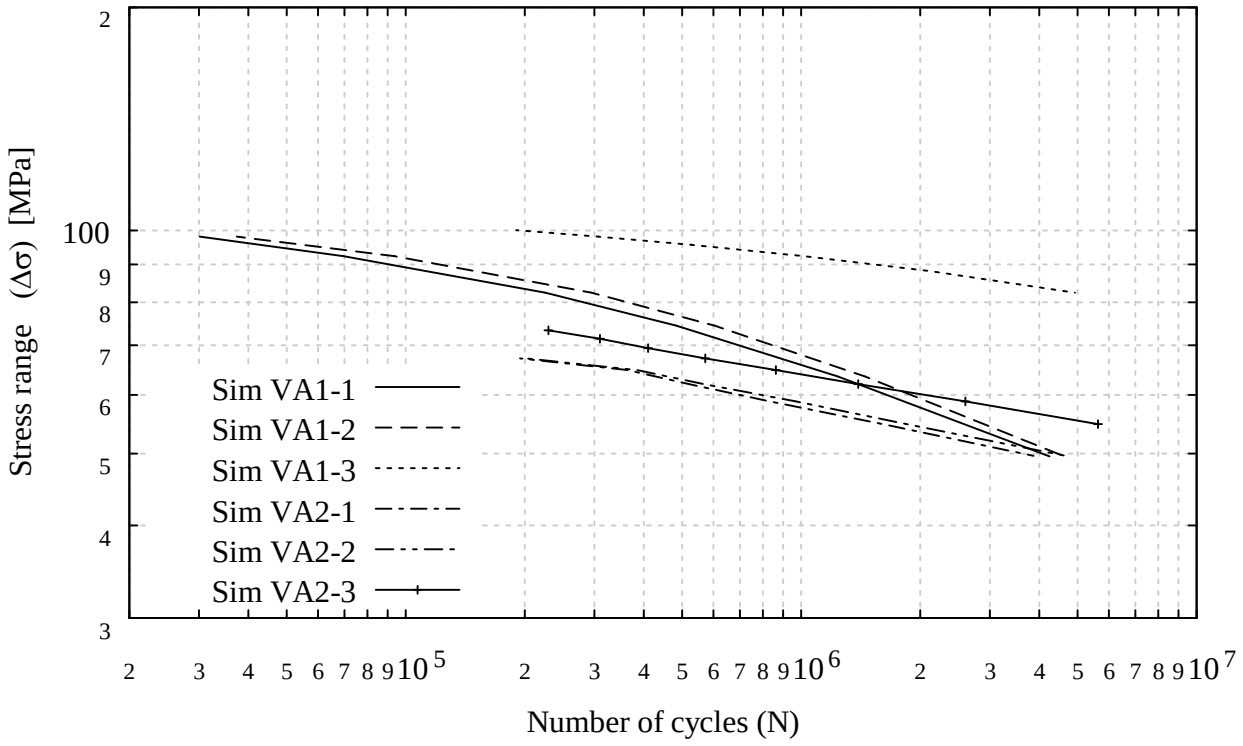

Figure 15: *S-N* Lines Obtained in Simulations for Variable Amplitude Loading with Load Histories from Strain Gauges No. 5 and 1

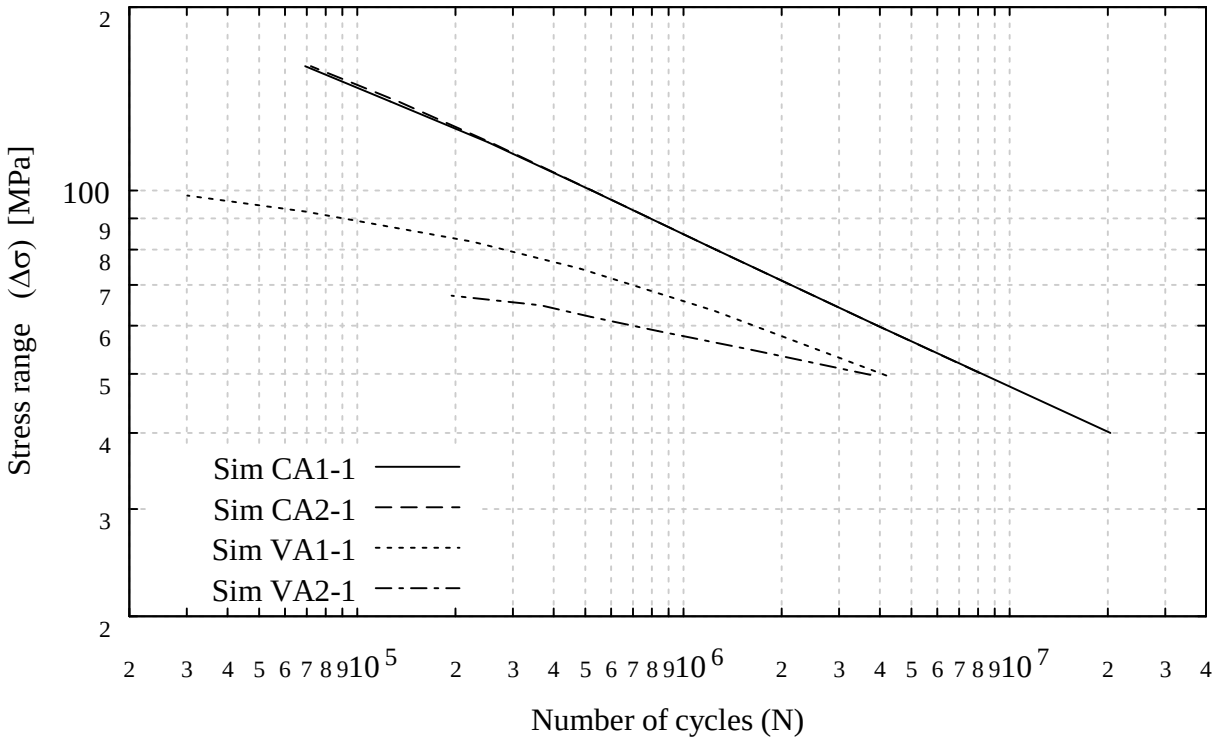

Figure 16: *S-N* Lines Obtained in Simulations for Constant Amplitude Loading and for Variable Amplitude Loading. Residual Stress, $\sigma_r = f_y$

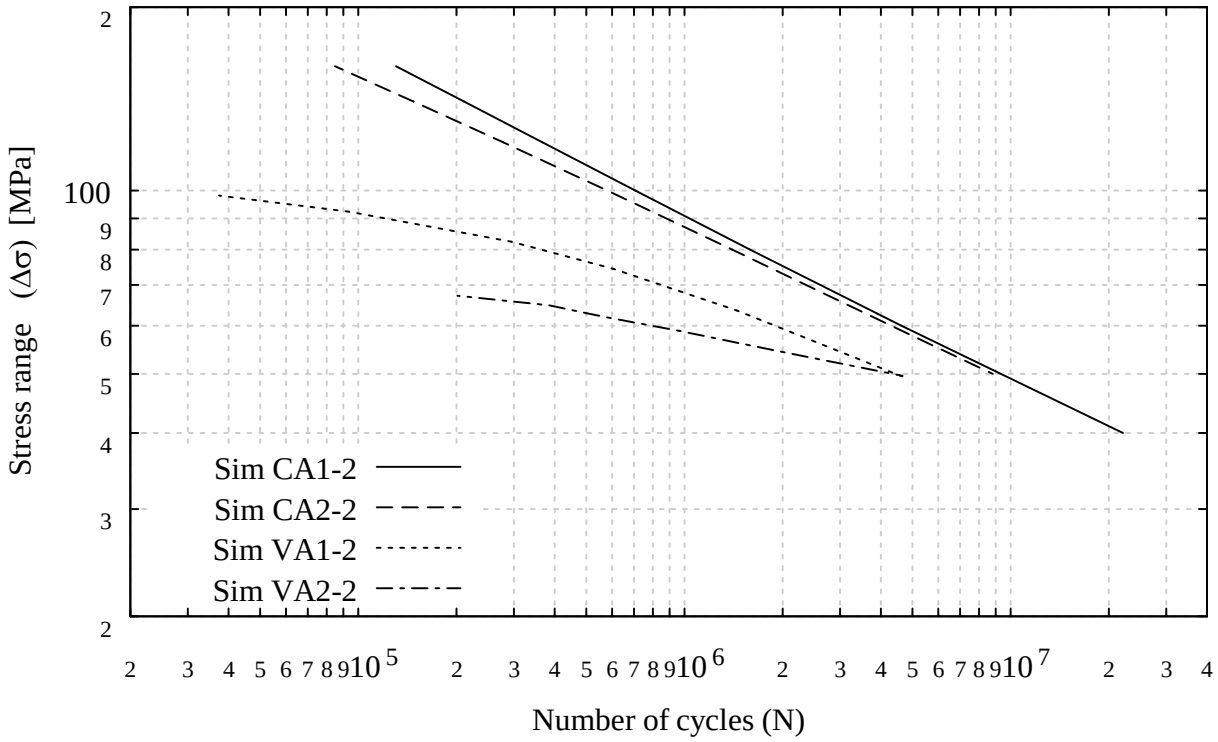

Figure 17: *S-N* Lines Obtained in Simulations for Constant Amplitude Loading and for Variable Amplitude Loading. Residual Stress, $\sigma_r = f_y/2$

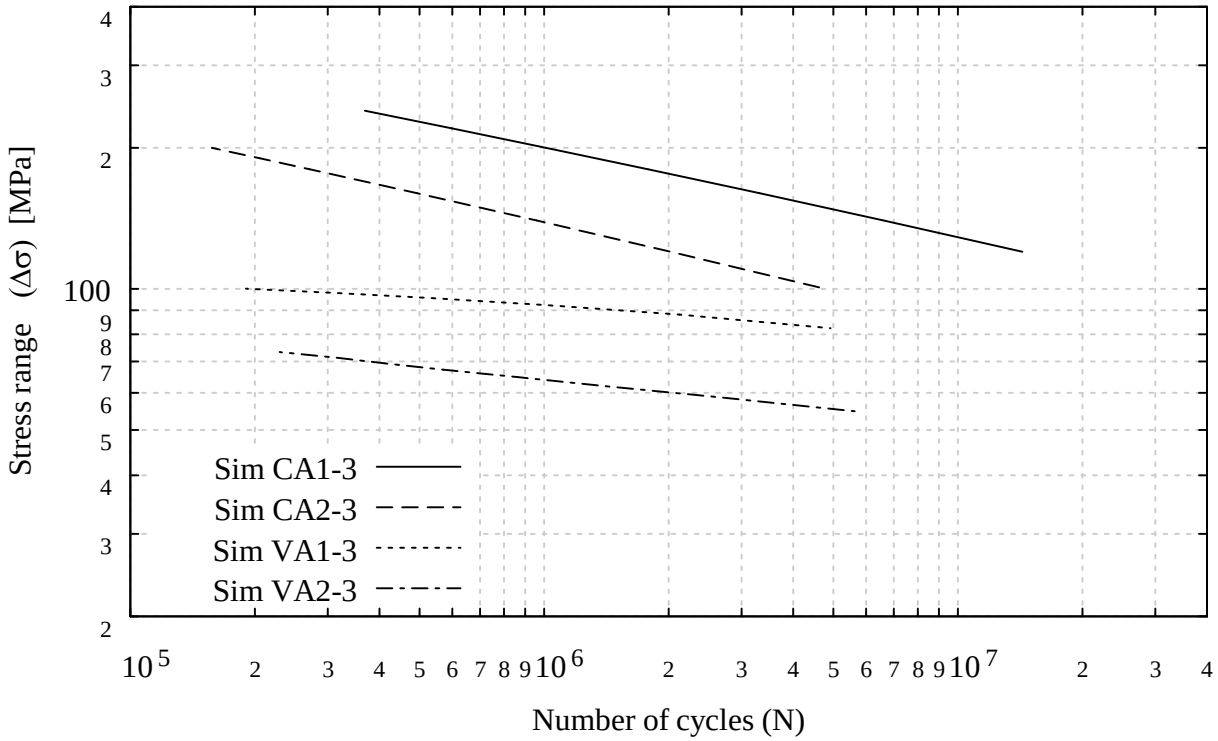

Figure 18: *S-N* Lines Obtained in Simulations for Constant Amplitude Loading and for Variable Amplitude Loading. Residual Stress, $\sigma_r = 0$

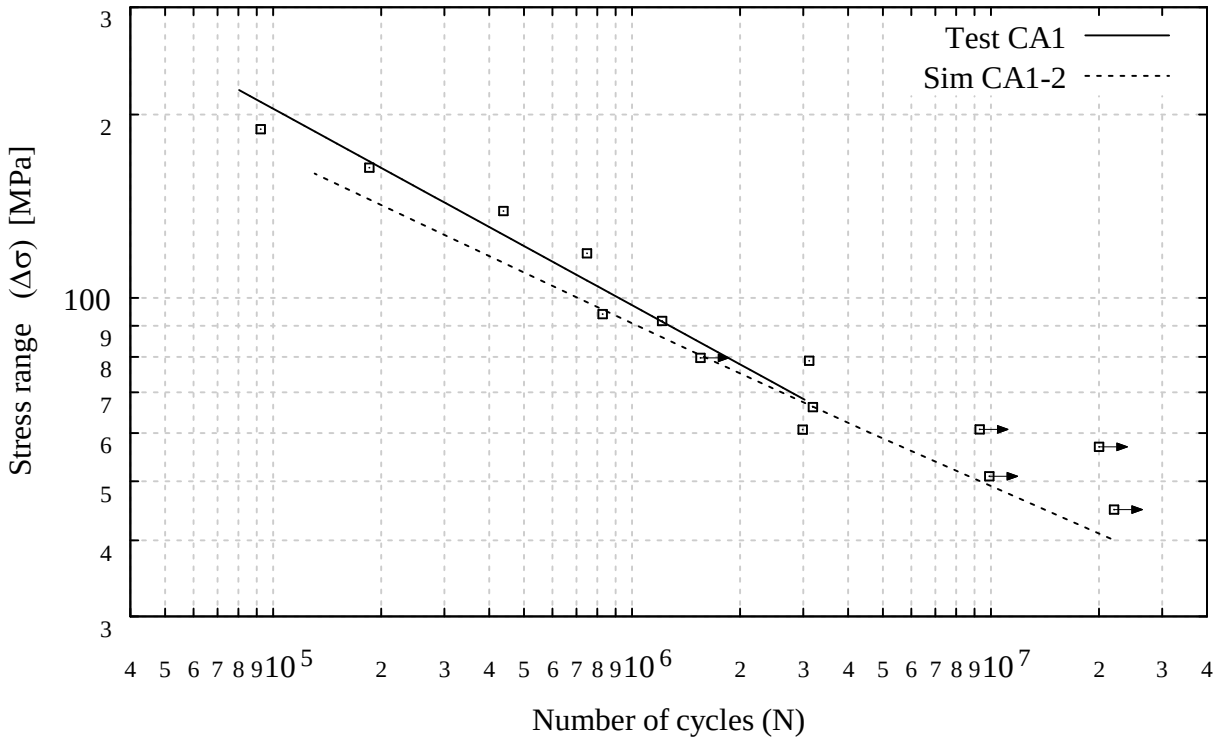

Figure 19: *S-N* Lines Obtained in Fatigue Tests and from Fracture Mechanics Analyses for Constant Amplitude Loading, *R* = -1

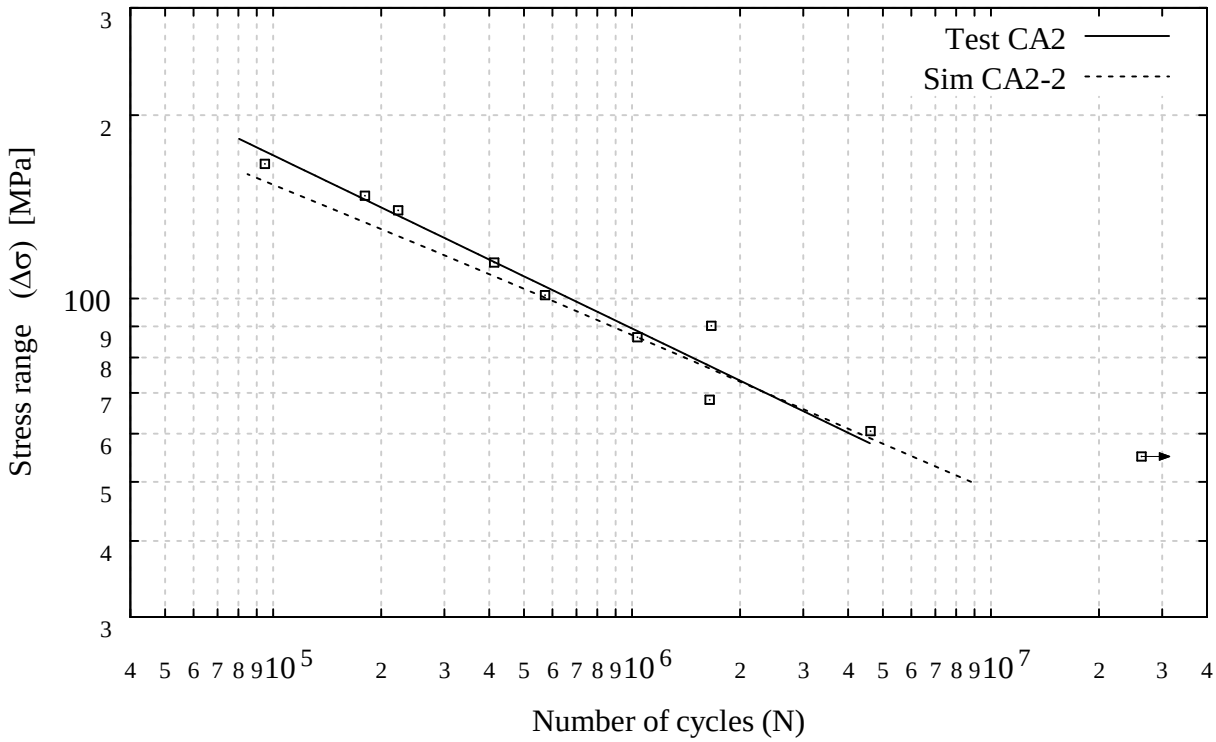

Figure 20: *S-N* Lines Obtained in Fatigue Tests and from Fracture Mechanics Analyses for Constant Amplitude Loading, *R* = -1/5

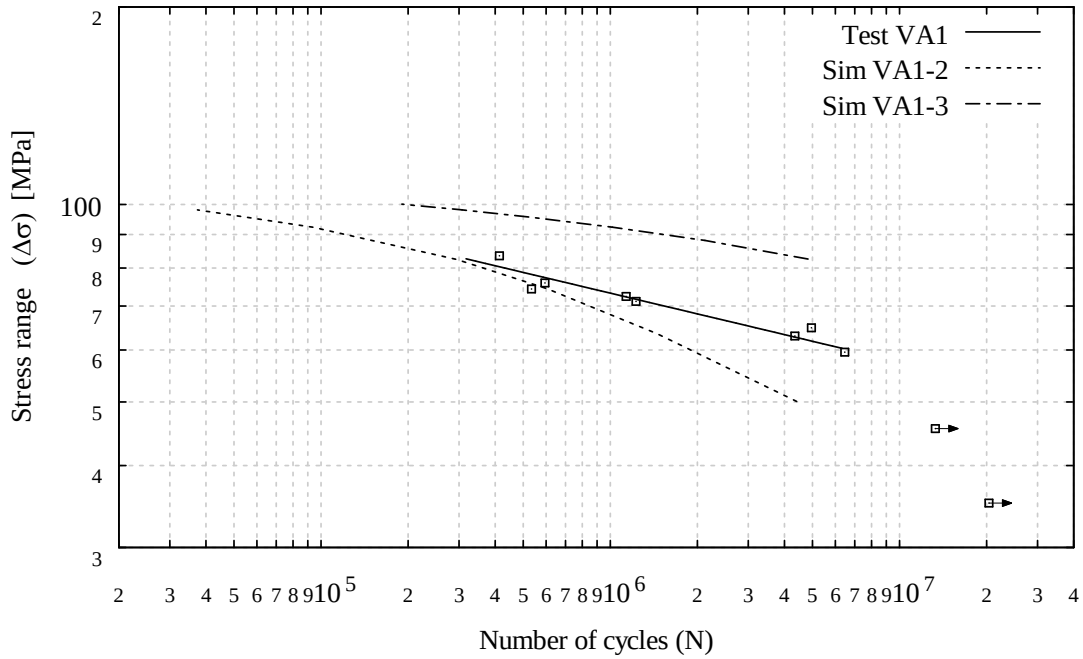

Figure 21: *S-N* Lines Obtained in Fatigue Tests and from Fracture Mechanics Analyses for Variable Amplitude Loading. Loading: Farø Bridges, Strain Gauge No. 5

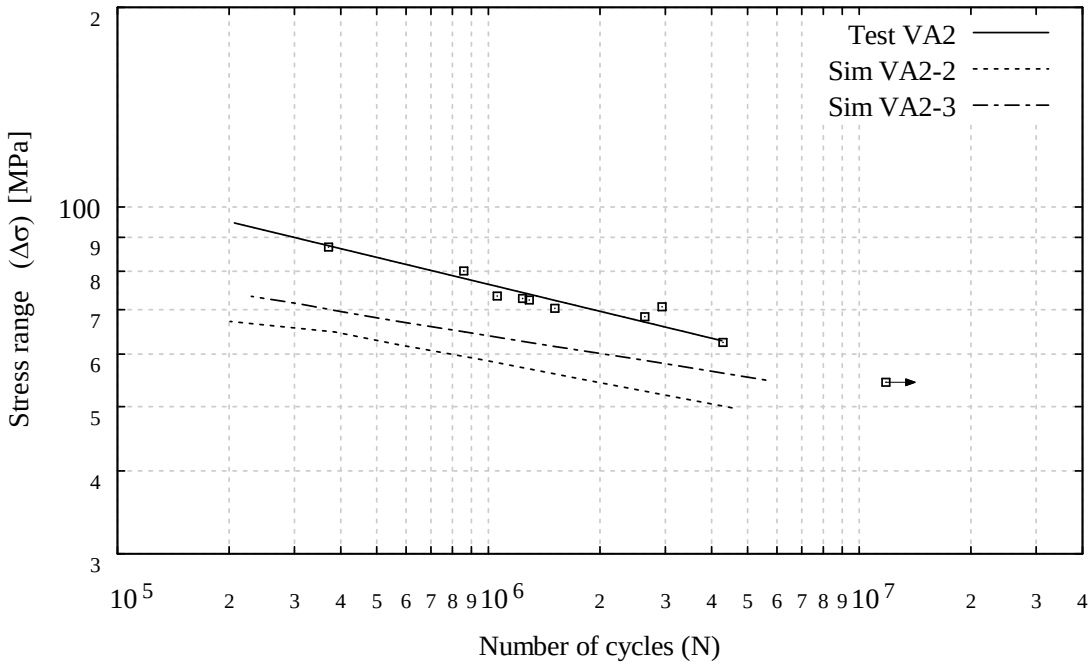

Figure 22: *S-N* Lines Obtained in Fatigue Tests and from Fracture Mechanics Analyses for Variable Amplitude Loading. Loading: Farø Bridges, Strain Gauge No. 1

Table 1: Characteristics of Load Histories Used

Load history (1)	*I* (2)	Root-mean square (RMS) (3)	Root-mean cube (RMC) (4)
Strain gauge No. 1	0.617	0.235	0.277
Strain gauge No. 5	0.793-0.834	0.245-0.272	0.287-0.321